Investigation of the effect of Ni substitution on the physical properties of $Ce(Cu_{1-x}Ni_x)_ySb_2$

2009 J. Phys.: Condens. Matter 21 056006

(http://iopscience.iop.org/0953-8984/21/5/056006)

J. Phys.: Condens. Matter **21** (2009) 056006 (7pp) doi:10.1088/0953-8984/21/5/056006

Investigation of the effect of Ni substitution on the physical properties of $Ce(Cu_{1-x}Ni_x)_ySb_2$

Dixie P Gautreaux[1], Michael Parent[1], Amar B Karki[2], David P Young[2] and Julia Y Chan[1,3]

[1] Department of Chemistry, Louisiana State University, 232 Choppin Hall, Baton Rouge, LA 70803, USA
[2] Department of Physics and Astronomy, Louisiana State University, Baton Rouge, LA 70803, USA

E-mail: jchan@lsu.edu

Received 28 May 2008, in final form 6 November 2008
Published 12 January 2009
Online at stacks.iop.org/JPhysCM/21/056006

Abstract

Single crystals of $Ce(Cu_{1-x}Ni_x)_ySb_2$ ($x = 0$, 0.25, 0.37, 0.46; $y \sim 0.7$) were synthesized using a flux growth method and crystallize in the tetragonal $P4/nmm$ space group with lattice parameters of $a \sim 4.4$ Å and $c \sim 9.8$ Å. The effects of Ni substitution on the magnetic and electrical transport properties are investigated. Three of the analogues (with $x = 0$, 0.37, and 0.46) show antiferromagnetic behavior while the $x = 0.25$ sample is paramagnetic down to 2 K. Field-dependent magnetization data as well as resistivities are presented. Positive magnetoresistance behaviors above 70% are observed for the analogues with $x = 0$, 0.37, and 0.46 at 3 K and up to 9 T. The La analogue $La(Cu_{0.2}Ni_{0.8})_ySb_2$, has been synthesized and large, positive magnetoresistance of ~300% is observed at 3 K and 9 T.

1. Introduction

Antimonide compounds have been a focus of many research groups because of the interesting structural features and physical properties they possess [1–4]. All analogues of $LnSb_2$ (Ln = La–Nd, Sm) show positive, linear magnetoresistance at 2 K [5]. Also of notable interest is $LaSb_2$, which has a positive, linear magnetoresistance below 10 K greater that 8500% with no signs of saturation up to 45 T [6]. Adopting a similar layered structure, $LnNi_{1-x}Sb_2$ (Ln = Y, Dy, and Ho) analogues have large positive magnetoresistance above 100% at 3 K [7]. Single crystalline $CeNiSb_2$ is reported to order ferromagnetically at 6 K and has a Sommerfeld coefficient (γ) of 55 mJ mol^{-1} K^{-2} [8]. It is important to note that the full structural determination has not been reported for $CeNiSb_2$, and the physical properties are similar to the fully characterized orthorhombic $CeNiSb_3$ which orders ferromagnetically at 6 K and has a Sommerfeld coefficient (γ) of ~50 mJ mol^{-1} K^{-2} [4, 9]. $CeMSb_2$ (M = Ni, Cu, Pd, and Ag) show dense Kondo behavior, and polycrystalline $CeNiSb_2$ shows an enhanced electron mass [10]. The magnetoresistance of polycrystalline $CeCuSb_2$ has been reported to be ~12.5% at 4.5 T and 4.5 K [11]. $CeCuSb_2$, both in the polycrystalline and single crystalline form, orders antiferromagnetically ~6.9 K [8, 10, 12–15]. $CeCuSb_2$ is also a heavy fermion with reported Sommerfeld coefficients (γ) of 94, 100, and 200 mJ mol^{-1} K^{-2} [8, 10, 14, 15].

In an effort to further determine structural stability of ternary Ce–Ni–Sb and Ce–Cu–Sb compounds, single crystals of various compositions of $Ce(Cu_{1-x}Ni_x)_ySb_2$ were grown. The crystal structure, elemental analysis, magnetic and transport properties of $Ce(Cu_{1-x}Ni_x)_ySb_2$ ($x = 0$, 0.25, 0.37, and 0.46) are reported herein.

2. Experimental details

2.1. Synthesis

High quality single crystals of $Ln(Cu_{1-x}Ni_x)_ySb_3$ were synthesized via flux growth by placing fragments of La or Ce rod (99.9% Alfa Aesar), Ni powder (99.999% Alfa Aesar), Cu powder (99.999% Alfa Aesar) and Sb shot (99.999% Alfa

[3] Author to whom any correspondence should be addressed.

Table 1. Crystallographic data for $Ln(Cu_{1-x}Ni_x)_ySb_2$ (Ln = La or Ce).

Nominal x	0	0.6	0.7	0.8	0.8
SC formula	$CeCu_{0.841}Sb_2$	$CeM_{0.707}Sb_2$	$CeM_{0.738}Sb_2$	$CeM_{0.665}Sb_2$	$LaM_{0.779}Sb_2$
Space group	$P4/nmm$	$P4/nmm$	$P4/nmm$	$P4/nmm$	$P4/nmm$
a (Å)	4.3650(2)	4.3790(2)	4.3780(3)	4.3800(2)	4.4000(2)
c (Å)	10.0010(6)	9.8480(7)	9.8160(8)	9.7900(6)	10.0490(9)
V (Å^3)	190.551(17)	188.842(18)	188.14(2)	187.815(17)	194.55(2)
Crystal size (mm^3)	0.05/0.13/0.17	0.05/0.13/0.13	0.05/0.10/0.13	0.08/0.13/0.15	0.05/0.08/0.10
Z	2	2	2	2	2
Temperature (°C)	25(2)	25(2)	25(2)	25(2)	25(2)
Density (g cm^{-1})	7.793	8.897	8.930	8.945	8.615
θ range (deg)	2.04–30.02	2.07–29.93	2.07–29.94	2.08–30.02	2.03–29.98
μ (mm^{-1})	30.989	36.104	36.239	36.302	34.326
R_{int}	0.0386	0.0420	0.0613	0.0379	0.0360
Collected reflections	541	466	356	489	460
Unique reflections	204	203	181	1	207
h	$-6 \leqslant h \leqslant 6$	$-6 \leqslant h \leqslant 6$	$-6 \leqslant h \leqslant 6$	$-6 \leqslant h \leqslant 6$	$-6 \leqslant h \leqslant 6$
k	$-4 \leqslant k \leqslant 4$	$-4 \leqslant k \leqslant 4$	$-4 \leqslant k \leqslant 3$	$-4 \leqslant k \leqslant 4$	$-4 \leqslant k \leqslant 4$
l	$-14 \leqslant l \leqslant 14$	$-10 \leqslant l \leqslant 13$	$-13 \leqslant l \leqslant 9$	$-13 \leqslant l \leqslant 2$	$-14 \leqslant l \leqslant 10$
$\Delta\rho_{max}$ (e Å^{-3})	3.005	3.4666	2.957	5.730	2.117
$\Delta\rho_{min}$ (e Å^{-3})	−1.709	−5.727	−5.933	−4.593	−1.959
Extinction coefficient	0.050(6)	0.051(7)	0.22(2)	0.090(16)	0.029(3)
$R[F^2 > 2\sigma(F^2)]$[a]	0.0379	0.0499	0.0466	0.0618	0.0286
$wR_2(F^2)$[b]	0.1007	0.1207	0.1207	0.1661	0.0732

[a] $R_1(F) = \sum \| F_0| - |F_c| \| \sum |F_0|$.
[b] $R_w(F_0^2) = \sum [w(F_0^2 - F_c^2)] / \sum [w(F_0^2)^2]^{1/2}$; $w = 1/[\sigma^2(F_0^2) + (0.0547P)^2 + 3.3374P]$, $w = 1/[\sigma^2(F_0^2) + (0.0840P)^2 + 3.5287P]$, $w = 1/[\sigma^2(F_0^2) + (0.0613P)^2 + 1.7761P]$, $w = 1/[\sigma^2(F_0^2) + (0.1045P)^2 + 7.0979P]$, $w = 1/[\sigma^2(F_0^2) + (0.0358P)^2 + 3.9432P]$ for $x = 0$, 0.6, 0.7, 0.8 (Ce), and 0.8 (La), respectively.

Aesar) in an alumina crucible. The nominal composition used was $1{:}x{:}1-x{:}20$ ($x = 0$, 0.6, 0.7, 0.8) for Ce:Ni:Cu:Sb, where excess Sb was included as the flux. For the La analogue, the nominal composition of 1:0.8:0.2:20 for La:Ni:Cu:Sb was used. Silica wool was placed on top of the crucible and the ampule was sealed under vacuum in a fused silica tube and placed in a furnace. The reaction vessel was heated to 1150 °C and held constant for 48 h, then cooled to 670 °C at a rate of 5 °C h^{-1}. Excess flux was removed by centrifugation. Single crystals were extracted with sizes up to $0.5 \times 1 \times 2$ mm^3 although the crystals tend to grow into larger, layered aggregates. The tetragonal plates are silver with a metallic luster. However, at lower concentrations of Cu, crystals gain a dull, blue-gray iridescence and begin to resemble crystals of $CeNiSb_3$ [4]. The crystals are stable in air over a period of months. It is important to note that under our growth conditions, where the nominal value of $x > 0.8$, single crystals of $CeNiSb_3$ were grown. This will be discussed more in depth in the structural analysis section.

2.2. Single crystal x-ray diffraction

A typical crystal with dimensions of $\sim 0.05 \times 0.10 \times 0.175$ mm^3 was mounted onto a glass fiber of a goniometer with epoxy and placed on a Nonius Kappa CCD x-ray diffractometer (Mo Kα = 0.710 73 Å). After choosing the tetragonal space group $P4/nmm$ (No. 129), the initial structural model was generated by SIR97 [16] and the model was then refined by direct methods using SHELXL97 [17]. Due to the similarity of Z for Ni and Cu, x-rays cannot accurately distinguish between the two. Therefore, the mixed transition metal site was refined as pure Cu for continuity and is designated as M. After refinement, the data were corrected for absorption and the displacement parameters were refined as anisotropic. An extinction coefficient was added and refined through multiple least squares cycles. A disagreeable thermal parameter for the transition metal site was observed and the site was allowed to be partially occupied. This is consistent with the partial transition metal occupancy observed in most other analogues of the $HfCuSi_2$ structure type. For simplicity, the exact partial occupancy will not be defined in the text for each compound as each value differs. It will be designated as y and the exact values will be listed in the crystallographic tables. Data collection parameters and crystallographic data are listed in table 1. Atomic coordinates, anisotropic displacement parameters, and site occupancies are provided in table 2.

2.3. Energy dispersive spectroscopy

Elemental analysis was performed on multiple single crystalline samples using the Hitachi S-3600N extra-large chamber variable pressure scanning electron microscope (VP-SEM) with an integrated energy dispersive (EDS) feature. Data were collected over a small flux-free area on the surface of the crystals using an accelerating voltage of 20 kV and 50 s acquisition times. This analysis was performed due to the similar x-ray scattering of Ni and Cu. X-ray diffraction cannot distinguish between elements with similar Z, and it is important to know the exact amounts of Ni and Cu in the sample. The transition metal site occupancy is consistent

Table 2. Atomic positions and displacement parameters for $Ln(Cu_{1-x}Ni_x)_ySb_2$ (Ln = La or Ce, M = mixture of Ni and Cu).

	Atom	Wyckoff site	x	y	z	U_{eq}(Å^2)[a]	Occupancy
$CeCu_{0.841}Sb_2$ $x = 0$	Ce1	2*c*	1/4	1/4	0.753 81(8)	0.0066(4)	1
	Cu1	2*a*	3/4	1/4	0	0.0103(8)	0.841(10)
	Sb1	2*c*	1/4	1/4	0.148 29(12)	0.0100(5)	1
	Sb2	2*b*	3/4	1/4	1/2	0.0079(4)	1
$CeM_{0.707}Sb_2$ $x = 0.6$	Ce1	2*c*	1/4	1/4	0.757 71(11)	0.0081(6)	1
	M1	2*a*	3/4	1/4	0	0.0083(10)	0.707(11)
	Sb1	2*c*	1/4	1/4	0.140 63(16)	0.0139(6)	1
	Sb2	2*b*	3/4	1/4	1/2	0.0092(6)	1
$CeM_{0.738}Sb_2$ $x = 0.7$	Ce1	2*c*	1/4	1/4	0.241 63(9)	0.0062(6)	1
	M1	2*a*	3/4	1/4	0	0.0103(10)	0.738(10)
	Sb1	2*c*	1/4	1/4	0.860 89(13)	0.0123(7)	1
	Sb2	2*b*	3/4	1/4	1/2	0.0075(7)	1
$CeM_{0.665}Sb_2$ $x = 0.8$	Ce1	2*c*	1/4	1/4	0.759 09(15)	0.0073(8)	1
	M1	2*a*	3/4	1/4	0	0.0063(14)	0.665(17)
	Sb1	2*c*	1/4	1/4	0.1367(8)	0.0136(8)	1
	Sb2	2*b*	3/4	1/4	1/2	0.0091(8)	1
$LaM_{0.779}Sb_2$ $x = 0.8$	La1	2*c*	1/4	1/4	0.756 41(11)	0.0067(4)	1
	M1	2*a*	3/4	1/4	0	0.0091(9)	0.779(10)
	Sb1	2*c*	1/4	1/4	0.139 48(14)	0.0129(4)	1
	Sb2	2*b*	3/4	1/4	1/2	0.0082(4)	1

[a] U_{eq} is defined as one-third of the trace of the orthogonalized U_{ij} tensor.

Table 3. EDS formula compositions for $Ce(Cu_{1-x}Ni_x)_ySb_2$.

Nominal composition, x	Single crystal formula	EDS formula
0.6	$Ce(M)_{0.707}Sb_2$	$Ce(Ni_{0.25}Cu_{0.75})_{0.69}Sb_{2.16}$
0.7	$Ce(M)_{0.738}Sb_2$	$Ce(Ni_{0.37}Cu_{0.63})_{0.74}Sb_{1.86}$
0.8	$Ce(M)_{0.665}Sb_2$	$Ce(Ni_{0.46}Cu_{0.54})_{0.67}Sb_{2.16}$

with the occupancy determined from single crystal x-ray diffraction data and formula compositions are located in table 3. Is is important to note that the nominal and exact Ni/Cu concentrations do not agree, however there is a systematic increase of Ni in both the nominal and exact compositions. From this point on, the actual EDS compositions will be used.

2.4. Physical property measurements

Magnetic measurements on single crystals of $Ce(Cu_{1-x}Ni_x)_ySb_2$ for the field applied along both the *c*- and *a*-axis were performed using a Quantum Design Physical Property Measurement System (PPMS). Temperature-dependent susceptibility data were measured with an applied field of 0.1 T from 2 K to 300 K. Magnetization as a function of field was measured at 3 K up to 9 T. The resistivity from 2 to 300 K and magnetoresistance at 3 K (up to 9 T) were measured using the standard four probe-AC method in the Quantum Design PPMS at ambient pressure.

3. Results and discussion

3.1. Structural changes

$Ln(Cu_{1-x}Ni_x)_ySb_2$ (Ln = La, Ce) crystallizes in the tetragonal space group $P4/nmm$ with the $HfCuSb_2$ structure type [18]. As indicated in tables 1 and 3, the nominal and exact compositions of Ni and Cu do not agree. However, there is a systematic increase of Ni in both the nominal and exact compositions. For consistency throughout this document, the compounds will be referred to by their actual compositions. We believe that there is a limit to the amount of Ni that can occupy the transition metal site when there is a large rare earth cation such as Ce present in the structure under our growth conditions. When too much Ni is added to the reaction mixture, the tetragonal structure can no longer be supported and the stable phase that forms is the α-$CeNiSb_3$ structure type [4]. This theory is supported by earlier work where pure $LnNiSb_2$ can only be formed in the presence of smaller rare earth cations (Gd–Er, Y) [7]. In the presence of larger rare earth ions such as Ce–Sm, the orthorhombic α-$LnNiSb_3$ structure is formed using the Sb flux growth method [4, 19]. We note that other experimental techniques such as arc-melting have yielded $LnNiSb_2$ (Ln = Pr, Nd, Sm) [12].

As previously stated, $Ln(Cu_{1-x}Ni_x)_ySb_2$ (Ln = La, Ce) crystallizes in the tetragonal space group $P4/nmm$. The structure consists of alternating layers of Sb2 square nets capped by Ln1 square antiprismatic layers and M1–Sb1 tetrahedral layers as shown in figure 1. The Ln atoms are coordinated to four Sb1 atoms from the M1–Sb1 tetrahedral layer and four Sb2 atoms from the net layer, forming a slightly distorted square antiprism. The M atoms are surrounded by four Sb1 atoms adopting a somewhat distorted tetrahedral geometry. This layered antimonide structure is similar to the orthorhombic $LnSb_2$ structure type which also includes alternating layers of Sb nets and $LnSb_8$ square antiprismatic layers [20].

Table 4 contains selected interatomic distances and Sb1–M1–Sb1 tetrahedral angles. As more Ni is introduced into the structure, the overall volume decreases which is expected, because Ni has a slightly smaller radius (1.15 Å) than Cu (1.17 Å). Also, the M1 tetrahedra show more distortion as the

Table 4. Selected interatomic distances (Å) and angles (deg) for $Ce(Cu_{1-x}Ni_x)_ySb_2$.

	x			
	0	0.25	0.37	0.46
Ce1–Sb1(x4)	3.2381(4)	3.2543(6)	3.2552(5)	3.2607(9)
Ce1–Sb2(x4)	3.2902(6)	3.3519(8)	3.3502(7)	3.3511(12)
M1–Sb1(x4)	2.6387(7)	2.5907(9)	2.5800(7)	2.5668(12)
Sb2–Sb2(x4)	3.086 52(14)	3.096 42(14)	3.0957(2)	3.097 13(14)
Sb1–M1–Sb1(x2)	111.61(4)	115.37(6)	116.09(5)	117.12(9)
Sb1–M1–Sb1(x4)	108.41(2)	106.60(3)	106.27(2)	105.79(4)

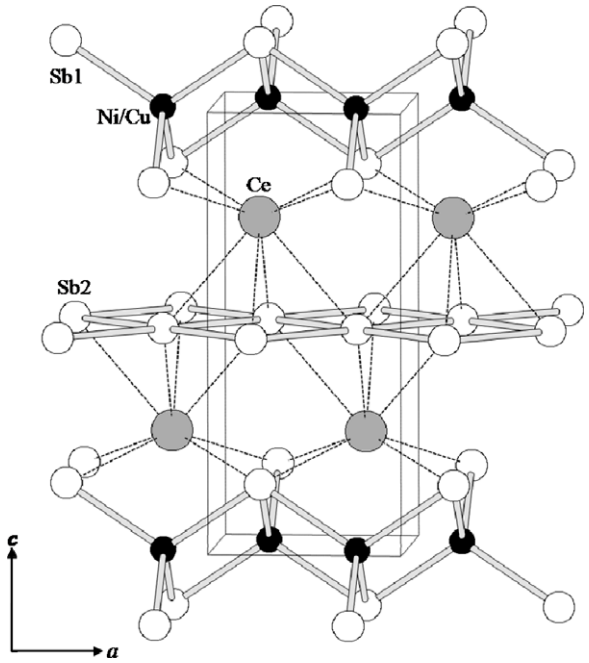

Figure 1. Crystal structure of $Ce(Cu_{1-x}Ni_x)_ySb_2$ as viewed down the b-axis where the gray shaded circles refer to the Ce atoms, the black circles refer to a mixture of Ni and Cu atoms and the white circles refer to the Sb atoms.

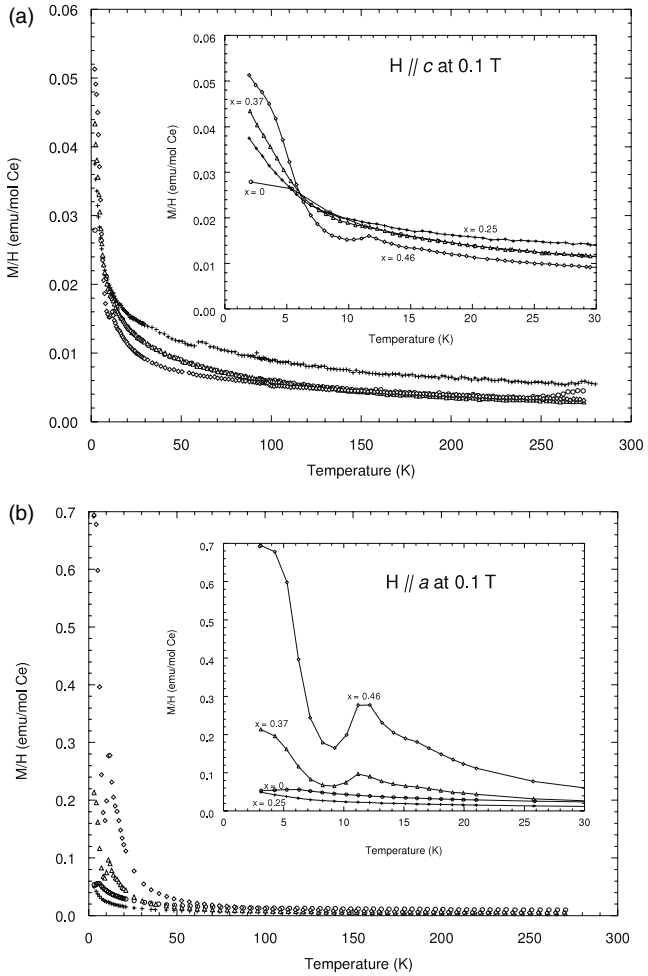

Figure 2. (a) Magnetic susceptibility of $Ce(Cu_{1-x}Ni_x)_ySb_2$ measured at a field of 0.1 T for $H \parallel c$ where the open circles, crosses, triangles, and open diamonds refer to $x = 0$, 0.25, 0.37, and 0.46 respectively. The inset displays a close-up of the susceptibility from 2–20 K. (b) Magnetic susceptibility as a function of temperature for the same samples for $H \parallel a$ (field along the ab-plane).

amount of Ni added to the structure is increased as indicated by the Sb1–M1–Sb1 angles listed in table 4. As expected, the M1–Sb1 distances decrease as a function of additional Ni introduced into the structure. The M1–Sb1 distances range from 2.6387(7) Å for pure $CeCu_{0.84}Sb_2$ to 2.5668(12) Å for $Ce(Cu_{0.54}Ni_{0.46})_{0.67}Sb_2$. The addition of Ni has very little effect on the Sb2 square nets as the Sb2–Sb2 distances show hardly any change (3.086 52(14)–3.097 13(14) Å), and there is no visible distortion as the Ni content increases.

3.2. Physical properties

The actual compositions of x will be used to describe the samples in this section and the value of y is ∼0.7. The magnetic susceptibility of $Ce(Cu_{1-x}Ni_x)_ySb_2$ ($x = 0$, 0.25, 0.37, 0.46) measured at an applied magnetic field of 0.1 T is shown in figure 2(a) for the field applied along the c-axis ($H \parallel c$). The Ni-substituted $Ce(Cu_{1-x}Ni_x)_ySb_2$ analogues ($x = 0.25$, 0.37) appear to be paramagnetic down to 2 K for this field orientation. For $Ce(Cu_{1-x}Ni_x)_ySb_2$ ($x = 0.46$), a sharp kink in the data is observed at ∼11 K. This feature is consistent with the onset of long-range antiferromagnetic order. $CeCu_{0.84}Sb_2$ ($x = 0$) orders antiferromagnetically at ∼5.5 K which is close to the literature reports of 6.9 K [8, 10, 12–15]. The effective moments for each sample were calculated using a modified Curie–Weiss equation, $\chi = \chi_0 + C/(T - \theta)$, where χ is the magnetic susceptibility, χ_0 is the temperature-independent contribution, C is the Curie constant, T is the temperature, and

Table 5. Summary of magnetic data for $Ce(Cu_{1-x}Ni_x)_ySb_2$ ($x = 0$, 0.25, 0.37, and 0.46). (Note: x = composition as obtained from elemental analysis.)

	x			
	0	0.25	0.37	0.46
$H \parallel c$				
T_N (K)	5.5	—	—	11.5
χ_0	0.007	0.001	0.001	0.001
C	0.790	0.738	0.768	0.790
θ (K)	−22	−45	−14	−28
μ_{exp} (μ_B)	2.51	2.43	2.48	2.51
$H \parallel ab$				
T_N (K)	6	—	11.5	11.5
χ_0	0.001	0.002	0.0006	0.001
C	0.610	0.891	0.720	0.680
θ (K)	−29	−42	−35	−62
μ_{exp} (μ_B)	2.21	2.60	2.40	2.33

θ is the Weiss constant. The high-temperature range of the data was fit (75–275 K). Experimental effective moments for $H \parallel c$ are 2.51, 2.43, 2.48, and 2.51 μ_B for $x = 0$, 0.25, 0.37, and 0.46. These values are close to the expected moment of 2.54 μ_B for the free Ce^{3+} ion. Curie temperatures of ∼−22, −45, −14, and −28 K were observed for compounds with $x = 0$, 0.25, 0.37, and 0.46, respectively, and indicate that there are antiferromagnetic correlations within the structures. Figure 2(b) shows the magnetic susceptibility as a function of temperature for the same samples for $H \parallel a$ (field along the ab-plane). For this orientation, antiferromagnetic transitions are enhanced and clearly visible ($T_N \sim 11$ K) in the samples for $x = 0.37$ and 0.46. The effective moments for each sample were also calculated using the modified Curie–Weiss equation. From the fits to the data, values for the effective moments were 2.21, 2.60, 2.40, and 2.33 μ_B for the $x = 0$, 0.25, 0.37, and 0.46, respectively—again close to the Ce^{3+} free ion moment. A summary of the magnetic data are located in table 5.

The magnetization at 3 K of $Ce(Cu_{1-x}Ni_x)_ySb_2$ ($x = 0$, 0.25, 0.37, and 0.46) as a function of field (up to 9 T) for $H \parallel c$ are shown in figure 3(a). The magnetization of pure $CeCu_{0.84}Sb_2$ is linear with field up to ∼6 T, consistent with antiferromagnetism below 6 K. None of the Ni-substituted compounds show any signs of saturation, appearing essentially paramagnetic with a fairly small moment at 9 T. The calculated saturation moment for a Ce^{3+} free ion is 2.14 μ_B. There are no signs of any hysteresis in any of the compounds measured. The magnetization of all analogues measured is small which suggests either a strong anisotropy or partial screening of the Ce moments by conduction electrons (Kondo screening).

Figure 3(b) shows the field-dependent magnetization for $H \parallel a$. For this orientation, the magnetization of $CeCuSb_2$ ($x = 0$), and the lowest Ni concentration ($x = 0.25$), remain essentially unchanged, with a slight enhancement in the moment. However, with the higher Ni concentration $x = 0.37$ and 0.46, a significant magnetic anisotropy is observed. In fact, several metamagnetic transitions are apparent for $x = 0.37$ occurring at approximately 0.45 and 1 T, and for $x = 0.46$, occurring at 0.5 and 1 T. When Ni is substituted into the series, the compounds become

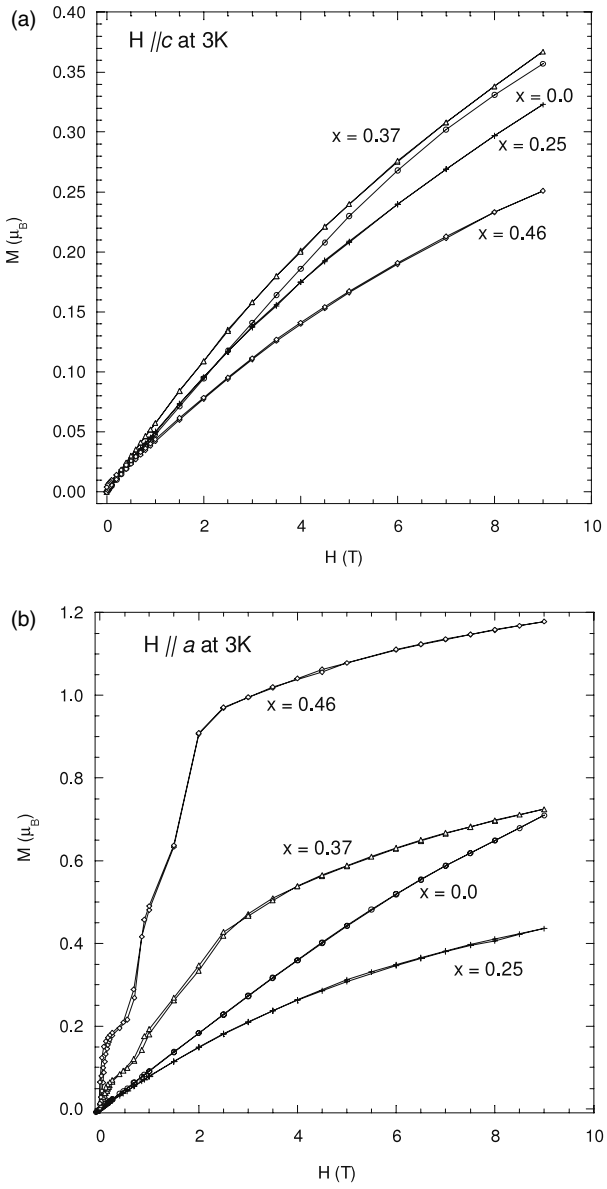

Figure 3. (a) Magnetism of $Ce(Cu_{1-x}Ni_x)_ySb_2$ measured at 3 K where the open circles, crosses, triangles, and open diamonds refer to $x = 0$, 0.25, 0.37, and 0.46 respectively for $H \parallel c$. (b) Shows the field-dependent magnetization for $H \parallel a$.

magnetically anisotropic, showing metamagnetic transitions for the field applied in the plane. The degree of this anisotropy seems to scale with the Ni concentration. The susceptibility data suggest that the magnetism is due solely to the local Ce moments, without magnetic contribution from the Ni atoms. The metamagnetic transitions could be due to spin-flip transitions if the Ce moments align ferromagnetically within the plane and antiferromagnetically between planes. However, detailed neutron scattering studies will be needed to confirm this. Furthermore, for $H \parallel a$, the magnetization of these samples with higher Ni concentration tends to saturate at higher magnetic field with a larger magnetization. For example, the sample for $x = 0.46$ has a high-field moment of ∼0.2 μ_B mol^{-1} Ce for $H \parallel c$ and 1.2 μ_B mol^{-1} Ce for $H \parallel a$. This suggests that the easy axis of magnetization is this series of compounds is along the a-axis.

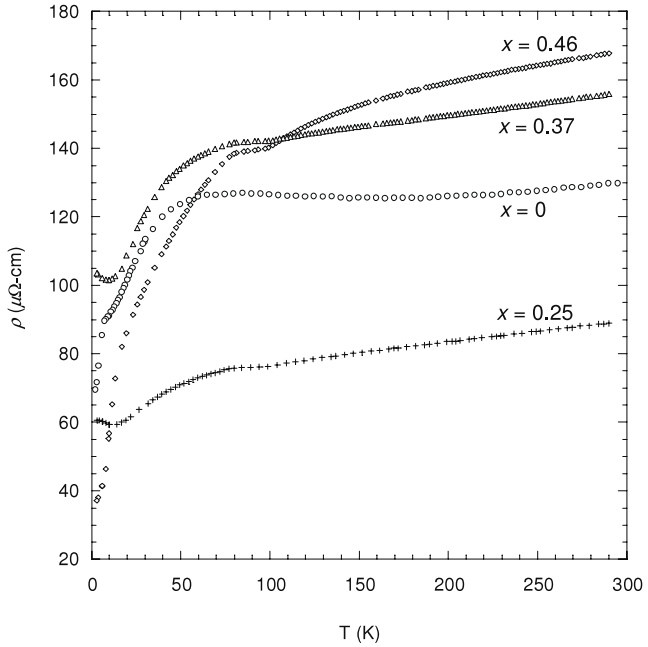

Figure 4. Resistivity of $Ce(Cu_{1-x}Ni_x)_ySb_2$ where the circles, crosses, triangles, and diamonds refer to $x = 0$, 0.25, 0.37, and 0.46, respectively.

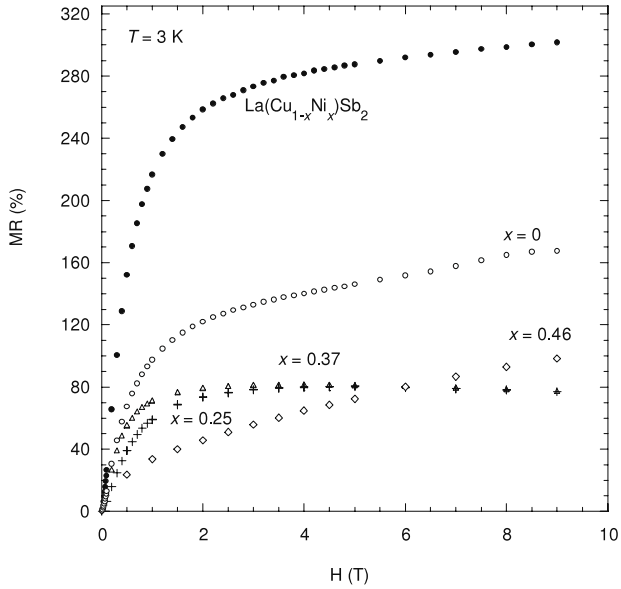

Figure 5. Magnetoresistance of $Ce(Cu_{1-x}Ni_x)_ySb_2$ and $La(Cu_{1-x}Ni_x)_ySb_2$ (nominal $x = 0.8$) measured at 3 K where the circles, crosses, triangles, and diamonds refer to the Ce analogues $x = 0$, 0.25, 0.37, and 0.46, respectively. The black circles refer to $La(Cu_{1-x}Ni_x)_ySb_2$.

Resistivity data were measured as a function of temperature for each analogue and are displayed in figure 4. All of the analogues display broad shoulders in the resistivity data as the temperature decreases which is indicative of Kondo behavior. Also, the classic upturn of the resistivity at low temperatures is seen for $Ce(Cu_{1-x}Ni_x)_ySb_2$ ($x = 0.25$ and 0.37). The resistivity data coupled with the screening of the Ce^{3+} moment seen in the magnetization data are signals that these compounds are more Kondo like. A sharp kink in the resistivity data for the $x = 0$ and 0.46 samples is observed at their ordering temperatures, consistent with a decrease in the spin-disorder scattering (figure 4, arrows).

The magnetoresistance at fields up to 9 T measured at 3 K is displayed in figure 5 for the Ce analogues and $La(Cu_{1-x}Ni_x)_ySb_2$ (nominal $x = 0.8$). The magnetoresistance for all analogues is larger than typical metals. The magnetoresistance of $CeCu_ySb_2$ increases quickly up to ∼1 T then increases at a slower rate up to ∼165% at 9 T. The magnetoresistance increases quickly up to ∼1 T then begins to saturate at 77%, and 80% for $x = 0.25$, and 0.37, respectively. The magnetoresistance for $Ce(Cu_{1-x}Ni_x)_ySb_2$ ($x = 0.46$) is similar to the other analogues up to ∼1 T, then the behavior deviates and increases with no signs of saturation up to 100% at 9 T. The magnetoresistance is not proportional to H^2 for all analogues, indicating that the magnetoresistive behavior is not classical. The magnetoresistance of $La(Cu_{1-x}Ni_x)_ySb_2$ (nominal $x = 0.8$) is significantly larger than the Ce analogues with the magnetoresistance saturating at ∼300%. This is not surprising as many La analogues have larger magnetoresistive behavior than other rare earth analogues, such as in $LaSb_2$ [5, 6].

In summary, we have synthesized high quality single crystals of tetragonal $Ce(Cu_{1-x}Ni_x)_ySb_2$ for $x = 0$, 0.25, 0.37, and 0.46. At higher Ni concentrations, the lower symmetry orthorhombic $CeNiSb_3$ structure is formed. Physical properties measurements show the samples to be metallic with a fairly large positive magnetoresistance at low temperature. A significant magnetic anisotropy develops in the Ni-substituted samples, with metamagnetic transitions appearing in the samples with higher Ni content. Strong antiferromagnetic correlations between lanthanide atoms persist in the Ni-doped samples, and the data suggest that the easy axis of magnetization in these materials lies along the a-axis. Detailed neutron scattering studies would be helpful in the solving the magnetic structure in this series.

Acknowledgments

JYC acknowledges support from the National Science Foundation (DMR grant no. 0756281) and the Alfred P Sloan Foundation and DPY also would like to acknowledge support from the National Science Foundation (DMR grant no. 049022).

References

[1] Mills A M, Lam R, Ferguson M J, Deakin L and Mar A 2002 *Coord. Chem. Rev.* **233/234** 207–22
[2] Sologub O and Salamakha P S 2003 *Handbook on the Physics and Chemistry of Rare Earths* vol 33, ed K A Gschneidner, J C G Bunzli and V K Pecharsky (Amsterdam: Elsevier)
[3] Kauzlarich S M 1996 *Chemistry, Structure, and Bonding in Zintl Phases and Ions* ed S M Kauzlarich (New York: VCH)
[4] Macaluso R T, Wells D M, Sykora R E, Albrecht-Schmitt T E, Mar A, Nakatsuji S, Lee H, Fisk Z and Chan J Y 2004 *J. Solid State Chem.* **177** 293–8
[5] Bud'ko S L, Canfield P C, Mielke C H and Lacerda A H 1998 *Phys. Rev.* B **57** 13624–38

[6] Young D P, Goodrich R G, DiTusa J F, Guo S, Adams P W, Chan J Y and Hall D 2003 *Appl. Phys. Lett.* **82** 3713–5
[7] Thomas E L, Moldovan M, Young D P and Chan J Y 2005 *Chem. Mater.* **17** 5810–6
[8] Thamizhavel A, Takeuchi T, Okubo T, Yamada M, Asai R, Kirit S, Galatanu A, Yamamoto E, Ebihara T, Inada Y, Settai R and Onuki Y 2003 *Phys. Rev.* B **68** 54427
[9] Siderov V A, Bauer E D, Lee H, Nakatsuji S, Thompson J D and Fisk Z 2005 *Phys. Rev.* B **71** 094422
[10] Muro Y, Takeda N and Ishikawa M 1997 *J. Alloys Compounds* **257** 23–9
[11] Lakshmi K V, Menon L, Nigam A K, Das A and Malik S K 1996 *Physica* B **223/224** 289–91
[12] Sologub O, Hiebl K, Rogl P, Noël H and Bodak O 1994 *J. Alloys Compounds* **210** 153–7
[13] Flandorfer H, Sologub O, Godart C, Hiebl K, Leith-Jasper A, Rogl P and Noel H 1996 *Solid State Commun.* **97** 561–5
[14] Koyama T, Matsumoto M, Wada S, Muro Y and Ishikawa M 2001 *J. Phys. Soc. Japan* **70** 3667–72
[15] Thamizhavel A, Okubo T, Yamada M, Galatanu A, Yamamoto E, Inada Y, Ebihara T and Onuki Y 2003 *Physica* B **327** 374–7
[16] Altomare A, Burla M C, Camalli M, Cascarno G L, Giacovazzo A, Guagliardi A, Moliterni A G G, Polidori G and Spagna R J 1999 *J. Appl. Crystallogr.* **32** 115–9
[17] Sheldrick G M 1997 *SHELXL97, Program for Refinement of Crystal Structures* (Germany: University of Gottingen)
[18] Andrukhiv L S, Lysenko L O, Yarmolyuk Y P and Hladyshevsky E I 1975 *Dopov. Akad. Nauk. Ukr. RSR* A **7** 645–8
[19] Thomas E L, Macaluso R T, Lee H, Fisk Z and Chan J Y 2004 *J. Solid State Chem.* **177** 4228–36
[20] Wang R and Steinfink H 1967 *Inorg. Chem.* **6** 1685–92